



# 1 On the measurement of stability parameter over complex 2 mountainous terrain

3 Elena Cantero<sup>1</sup>, Javier Sanz<sup>1</sup>, Fernando Borbón<sup>1</sup>, Daniel Paredes<sup>2</sup>, Almudena García<sup>3</sup>

4  
5 <sup>1</sup>National Renewable Energy Centre (CENER), Sarriguren, Spain

6 <sup>2</sup>Iberdrola, Madrid, Spain

7 <sup>3</sup>Smart Cities Institute, Universidad Pública de Navarra (UPNA), Spain

8 *Correspondence to: Elena Cantero (ecantero@cener.com)*

9 **Abstract.** Atmospheric stability has a significant effect on wind shear and turbulence intensity, and these variables,  
10 in turn, have a direct impact on wind power production and loads on wind turbines. It is therefore important to know  
11 how to characterize atmospheric stability in order to make better energy yield estimation in a wind farm.

12 Based on research grade meteorological mast at Alaiz (CENER's Test Site in Navarre, Spain) named MP5, this work  
13 compares and evaluates different instrument set-ups and methodologies for stability characterization. The Obukhov  
14 parameter  $\zeta = z/L$ , which can be measured locally with the use of a sonic anemometer, and bulk Richardson number  
15 have been studied. The methods are examined considering their theoretical background, implementation complexity,  
16 instrumentation requirements, and practical use in connection with wind energy applications.

17 Bulk Richardson number, which is based on one height wind speed measurement and two temperature  
18 measurements, is sometimes calculated using values from any two temperature levels without taking into account  
19 that one of the measurements would be representative of surface conditions. With the data available in MP5, it will  
20 be shown how this approximation is not correct to obtain an adequate stability characterization.

## 21 1. Introduction

22 The vertical wind profile and the turbulence intensity in the atmospheric boundary layer (ABL) are two of  
23 the features that most affect the wind energy generation. The wind profile because given the growing hub heights  
24 and rotor sizes of the modern wind turbines it affects the wind turbine production and loads; and the turbulence  
25 intensity because it induces loads that the wind turbine will support over its design lifetime. Despite the fact that  
26 the IEC standard (IEC61400-1 (ED4) 2019, 2019) specifies a power law vertical model independent of  
27 atmospheric stability to perform load calculations, the dependence of this and, in turn, the turbulence intensity  
28 with atmospheric stability is widely demonstrated (Lange et al., 2004b; Peña y Hahmann, 2012; Stefan Emeis,  
29 2013). In addition several studies have demonstrated the impact of atmospheric stability on wind resource  
30 assessment (Lange et al., 2004a), wind turbine power curves and AEP calculations (Martin et al., 2016; Schmidt  
31 et al., 2016); wind turbine loads (Kelly et al., 2014; Sathe et al., 2013) and wind turbine wakes (Abkar y Porté-  
32 Agel, 2015; Hansen et al., 2010; Macheaux et al., 2016). This is why the wind industry is developing models and  
33 methods to include the effect of atmospheric stability in the layout design and energy yield assessment. These  
34 methodologies and models require the characterization of the probability distribution of atmospheric stability at  
35 each site. Therefore different methods and parameter are used to describe atmospheric stability without an  
36 industry-wide convention about which one is the most appropriate.

37 According to Monin and Obukhov similarity theory (MOST) (Foken, 2006; Monin y Obukhov, 1954) stability  
38 can be estimated in terms of inverse of Obukhov length that can be calculated with vertical fluxes of heat and  
39 momentum obtained with the eddy covariance method. To obtain the necessary high-frequency measurements of  
40 wind speed vector components and temperature, sonic anemometers are used, which is why this calculation method  
41 is called "sonic method".

42 Another measure for stability is the Richardson number that as Bardal (Bardal et al., 2018) explains according to  
43 Stull book (Stull, 1989) has several formulations: the flux Richardson number, gradient Richardson number and  
44 bulk Richardson number. The latter is based on one height wind speed measurement and two temperature  
45 measurements, one from the air at one height and the other from the ground or water surface.

46 In the wind energy context some studies have been done about how to measure the stability and their influence in  
47 the turbulence intensity and vertical wind profile. However, most of these studies have been carried out in offshore



48 sites (Peña y Hahmann, 2012; Sanz Rodrigo et al., 2015; Sathe et al., 2011) finding relationships (Grachev y Fairall,  
49 1997) between the Obukhov length and the Richardson bulk number that, facilitate the characterization of stability  
50 without the need of sonic anemometer. This is convenient to avoid the added complexity and cost of these  
51 instruments in long-term site assessment campaigns.

52 For onshore sites there are few studies that analyse how to characterize atmospheric stability and those that exist  
53 are on simple topography in coastal areas (Bardal et al., 2018).

54 Although the behaviour of wind flow over complex terrain is widely studied, as Finnigan summarizes in  
55 (Finnigan et al., 2020) and there are recent publications about the influence of atmospheric stability in wind farms  
56 located in complex terrain (Han et al., 2018; Radünz et al., 2020, 2021); there are no references that analyse in detail  
57 how to characterize atmospheric stability according to different instrumentation requirements.

58 Measuring atmospheric stability in complex terrain has some challenges (compared to flat terrain), one of them  
59 is the fact that the MOST is developed for horizontally homogeneous and flat terrain and in complex terrain vertical  
60 wind speed can be due to stability or sloping terrain, therefore, vertical fluxes will be “contaminated” by terrain  
61 effects. This can be mitigated by using good measurement practices (data quality, coordinate systems and post  
62 processing options) (Stiperski y Rotach, 2015).

63 This study presents atmospheric stability characterization from one mountainous site obtained using two  
64 methods: sonic method and the Richardson bulk number. Measurements of different heights have been used to see  
65 the influence of this parameter on the results

66 The place used in this study meets the characteristics of a typical complex terrain site for wind energy  
67 deployment. The 118 m high MP5 reference meteorological mast, as is explained in other articles by Sanz  
68 Rodrigo et al., 2013) and Santos (Santos et al., 2020), is equipped with wind (cup and 3D sonic anemometer) and  
69 temperature measurements distributed along six vertical levels: 2, 40, 80, 90, 100 and 118 m above the ground level  
70 (a.g.l), enabling the comparison between Richardson bulk number and the sonic method to evaluate atmospheric  
71 stability.

72 Special focus is given to explaining the post-processing methodologies to derive stability from raw data  
73 considering fast-response sonic anemometer in a complex terrain.

## 74 2. Atmospheric stability definitions

### 75 2.1 The Obukhov length

76 Monin and Obukhov (M-O) (Monin y Obukhov, 1954) introduced the Obukhov length  $L$  to characterize atmospheric  
77 stability, which is proportional to the height above the surface at which the production of turbulent energy from  
78 buoyancy dominates over mechanical shear production of turbulence (Stull, 1989), and it is defined as:

$$L = -\frac{u_*^3}{\kappa \frac{g}{\Theta_0} \overline{w\theta}}$$

**Equation 1**

79 Where  $g$  is the acceleration due gravity,  $\kappa = 0.41$  is the von Karman constant,  $u^*$  is the friction velocity,  $\Theta_0$  is the  
80 surface potential temperature and  $\overline{w\theta}$  is the heat flux. The dimensionless height  $\zeta = z/L$  is used as stability  
81 parameter, where  $\zeta < 0$  indicates unstable,  $\zeta > 0$  stable and  $\zeta = 0$  neutral conditions.

82 Table 1 shows the Sorbjan & Grachev (Sorbjan y Grachev, 2010) stability classification, they identify four  
83 regimes in the stable boundary layer. This classification is followed by Sanz (Sanz Rodrigo et al., 2015) assuming a  
84 symmetric classification in the unstable range. Sanz *et al.* shift the "extremely un/stable" regime limit to  $|\zeta| = 1$  in  
85 order to avoid contamination of the large scatter found in the high ends of the scale to the "very un/stable" class. An  
86 additional limit is added at  $|\zeta|=0.2$  to give higher resolution in the most frequent stability range. For consistency, we  
87 shall adopt the same classification used in (Sanz Rodrigo et al., 2015) to facilitate the comparison with offshore  
88 conditions.

89  
90  
91  
92



93 **Table 1 Classification of atmospheric stability (symmetric for the unstable range)** (Sorbjan y Grachev, 2010).  
 94

Stability Class	Stability parameter $\zeta = z/L$
near-neutral (n)	$0 < \zeta < 0.02$
weakly stable (ws)	$0.02 < \zeta < 0.2$
stable (s)	$0.2 < \zeta < 0.6$
very stable (vs)	$0.6 < \zeta < 1$
extremely stable (xs)	$\zeta > 1$

95  
 96 Using sonic anemometers and eddy covariance technique, the Obukhov length can be obtained. In this way,  
 97 stability is evaluated locally based on turbulent fluxes averaged over periods from minutes to one hour to integrate  
 98 the kinetic energy in the microscale turbulence range.

99 Sonic anemometer can be used in complex terrain to derive the local Obukhov length. Following the planar fit  
 100 method of Wilczak *et al.* (Wilczak *et al.*, 2001), momentum fluxes should be calculated in the mean streamline plane  
 101 and heat fluxes in the true vertical coordinate system. If the streamline plane can be known a priori, from a wind  
 102 direction sector with uniform slope, the planar fit method can be used to infer the mounting tilt angle and correct for  
 103 it to reduce the uncertainty on the vertical fluxes.

## 104 2.2 Bulk Richardson number

105 The bulk Richardson number  $Ri_b$  is a form of the Richardson number that is widely used for characterizing stability  
 106 for its simplicity, defined in terms of a (potential) temperature difference and a single velocity level:

$$Ri_b = -\frac{gz\Delta\theta}{\theta_0\overline{u^2}} \quad \text{Equation 2}$$

107 Where, as propose Sanz *et al.* in (Sanz Rodrigo *et al.*, 2015), the height  $z$  is taken here as the mean height  
 108 between the two levels of temperature and  $\Delta\theta$  is derived from the water-air or surface-air temperature difference.

109 As Bardal *et al.* propose in (Bardal *et al.*, 2018) the general empirical relations from Businger *et al.* (Businger *et al.*,  
 110 1971) slightly modified by Dyer (Dyer, 1974) have been used to relate  $\zeta$  with the Rib:

$$\xi = \begin{cases} Ri_b, & Ri_b < 0 \\ \frac{Ri_b}{1-5Ri_b}, & 0 < Ri_b < 0.2 \end{cases} \quad \text{Equation 3}$$

112 Alternatively  $Ri_b$  can be used directly to do a stability classification, according to Mohan (Mohan, 1998) which  
 113 classification is used in literature (Ruishi y Bossanyi, 2019), based on seven classes of stability (Table 2).

114 **Table 2 Classification of atmospheric stability (Mohan, 1998).**  
 115

Stability Class	Stability parameter $Ri_b$
Very unstable	$Rib < -0.023$
Unstable	$-0.023 \leq Rib < -0.011$
Weakly unstable	$-0.011 \leq Rib < -0.0036$
Neutral	$-0.0036 \leq Rib < 0.0072$
Weakly stable	$0.0072 \leq Rib < 0.042$
Stable	$0.042 \leq Rib < 0.084$
Very stable	$Rib \geq 0.084$

## 116 3. The Alaiz site

117 The MP5 mast is located (42°41.7' N, 1°33.5' W) at the top of Alaiz mountain in the region of Navarre (Spain),  
 118 around 15 km SSE from Pamplona in the CENER's experimental wind farm. The prevailing wind directions are  
 119 from the North and from the South. To the North there is a large valley at around 700 m lower altitude. To the  
 120 South, complex terrain is found with the presence of some wind farms; the closest one situated 2 km behind the row  
 121 of six wind turbine stands of the test site (see Figure 1). Besides MP5 meteorological mast there are four other  
 122 reference met masts (MP0, MP1, MP3 and MP6), all of them 118 m tall.

123 The test site started operating in 2009 with the site calibration procedures. The first wind turbines were installed  
 124 in the summer of 2011. The standard configuration of each mast is designed for multi-megawatt wind turbine testing



125 and includes sonic and cup anemometer, wind vanes and temperature/humidity measurements. Replicated cup  
126 anemometers are situated 2 m below the reference ones.

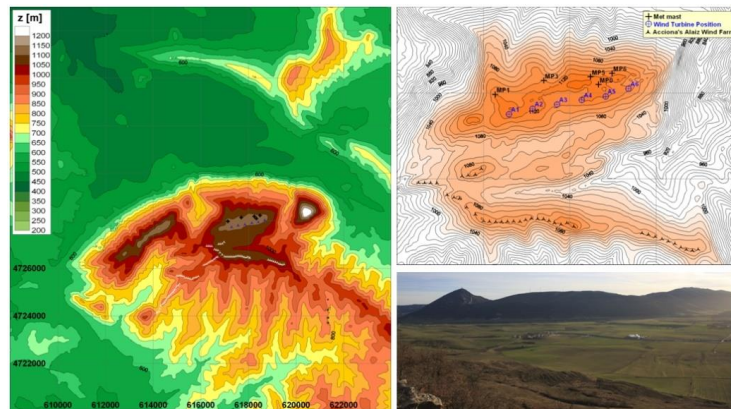
127 The mast MP5 is 118 m high lattice permanent mast with nine measurement levels with booms oriented to the  
128 West (263°) and the East (83°). Wind speed and wind direction are measured at five levels (118, 102, 90, 78 and 40  
129 m) with cups anemometer (oriented to the West) and wind vanes (oriented to the East); while sonic anemometer are  
130 installed at 115.5, 75.5 and 39.5 m (oriented to the West). Temperature and relative humidity are measured at five  
131 levels (113, 97, 81, 38 and 2 m) and pressure at 2 m high.

132 The instrumental set-up is compliant with IEC 61400-12-1(IEC61400-12-1 (ED1) 2005-12, 2005) with  
133 MEASNET cup anemometer calibration (Measnet, 2009) and with ENAC accreditation according to UNE-EN  
134 ISO/IEC 17025.

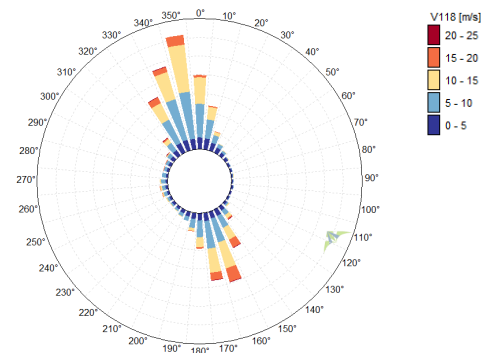
135 The data acquisition system consist in a real-time controller CompactRIO from National Instruments with 128  
136 MB DRAM and 2 GB storage embedded in a chassis in connection with 8 modules of digital and analogical data  
137 acquisition. All connected to an Ethernet network.

138 The rate sample is 5 Hz for cup anemometer (Vector A100LK) and 20 Hz for sonic anemometer (METEK USA-  
139 1), wind vanes (Thies Compact), pressure (Vaisala PTB100A), and humidity temperature sensor (Ammonit P6312).

140 Figure 2 shows the wind rose at the MP5 site, from the period between July 2014 to June 2015. It presents a  
141 bidirectional wind climate, with prevailing winds from the north-northwest sector (330–360, 32% of total) and the  
142 south southeast sector (150–180, 28% of total).



143  
144 **Figure 1** Alaiá elevation map, close-up of the test site and view from the upstream ridge to the North.



145 **Figure 2** Wind rose of 10 min wind speeds observed by MP5 at 118m for the reference period (July 2014–June 2015).



## 146 4. Methodology

147 In the present work, a one year period (1st July 2014 to 30th June 2015) is analyzed. Measurements from the sonic  
148 anemometer at 115.5, 75.5 and 39.5 m are used to calculate de Obukhov length  $L$ , while conventional sensors (wind  
149 direction, relative humidity, air pressure and temperature) are used to estimate the bulk Richardson number.

### 150 4.1 Data quality control

151 Before calculating stability parameter all data are checked for data quality.

152 Data from conventional sensors (wind direction, relative humidity, air pressure and temperature) have been  
153 processed following Brower (Brower, 2012). It consists on checking the completeness of the collected data and  
154 applying several test (range, relational and trend). After filtering for quality-control purposes, the conventional  
155 sensors provide horizontal wind speeds, directions, relative humidity, pressures and temperatures availabilities  
156 greater than 85% at all levels during the evaluation period.

157 For sonic anemometer there are a lot of procedures (Aubinet et al., 2012) and test criteria for quality control of  
158 turbulent time series and studies about the impact in the results of this procedures (Stiperski y Rotach, 2015).

159 High-frequency raw data often contain impulse noise, that is, spikes, dropouts, constant values, and noise. Spikes  
160 in raw data can be caused by instrumental problems, such as imprecise adjustment of the transducers of ultrasonic  
161 anemometer, insufficient electric power supply, and electronic noise, as well as by water contamination of the  
162 transducers, bird droppings, cobwebs, etc., or rain drops and snowflakes in the path of the sonic anemometer.

163 Several spikes in wind speed have been detected in the raw sonic anemometer data. Therefore, a de-spiking filter  
164 is applied based on the change in wind speed from each data point to the next and taking into account the physical  
165 limits according to sensor specifications. Data points are removed if they are preceded and followed by changes  
166 exceeding the lowest 99% of all changes. After filtering the spikes, the sonic anemometer provide wind speed and  
167 temperature availabilities greater than 80% in the three sonic anemometer.

### 168 4.2 Eddy Covariance method

169 The operating principles of sonic anemometer are described by different authors (Aubinet et al., 2012; Cuerva et al.,  
170 2003; Kaimal y Businger, 1963; Kaimal, 1994; Schotanus et al., 1983). The sonic anemometer output provides three  
171 wind components in an orthogonal axis system and sonic temperature. The relation between sonic temperature and  
172 absolute real temperature is given by Kaimal & Gaynor (Kaimal y Gaynor, 1991).

173 High frequency data from sonic anemometer have been processing to obtain 10 minutes databases that include  
174 turbulent fluxes of energy, mass, and momentum with the eddy covariance technique (Aubinet et al., 2012)(Burba,  
175 2013; Burba y Anderson, 2010; Geissbühler et al., 2000).

176 The main requirements for instruments and data acquisition systems used for eddy covariance data are their  
177 response time to solve fluctuations up to 10 Hz. This means that the sampling frequency has to be high enough to  
178 cover the full range of frequencies carrying the turbulent flux, leading usually to a sampling rate of 10–20 Hz. In the  
179 test case in this report 20 Hz is the sample rate for the sonic anemometer.

180 The transformation of high-frequency signals into means, variances, and covariances requires different steps  
181 (Aubinet et al., 2012; Stiperski y Rotach, 2015), in this study the next steps has been proposed:

- 182 1. Quality Control of raw data, explained in point 4.1.2
- 183 2. Coordinate Rotation, transformation of coordinate systems, from the original axes based on the anemometer  
184 output to the streamline terrain-following system, based on the Planar Fit Method (PFT) (Richiardone et al.,  
185 2008; Wilczak et al., 2001). Figure 3 shows the steps to rotate the axes from mounting coordinates to streamline  
186 coordinates.

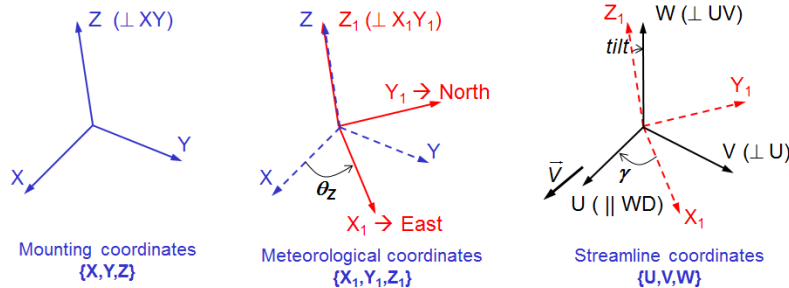


**Figure 3 Schematic description for the rotation process.**

187

188 3. Variance and Covariance Computation, apply eddy covariance technique for calculation of vertical turbulent  
 189 fluxes (heat and momentum). It corresponds to the calculation of the covariance of the fluctuations of the vertical  
 190 velocity with the quantity  $\Phi$  (temperature for heat, velocity components for momentum).

$$F_{\phi} = \overline{w'\phi'} = \overline{w\phi} - \overline{w}\overline{\phi} = \frac{1}{N-1} \left[ \sum w'\phi' - \frac{1}{N} (\sum w') (\sum \phi') \right] \quad \text{Equation 4}$$

191

192 N denotes the number of samples considered for the short averaging period T over which the flux is  
 193 calculated (from 5 to 60 min). N has to be long enough to ensure statistical convergence and short enough to assume  
 194 stationarity (in complex terrain difficult to fulfil both criteria). In this work a 10 minutes averaging period has been  
 195 selected.

196 In the MP5's sonic anemometer, at 115.5, 75.5 and 39.5 m height, moreover the temperatures, the variables  
 197 recorded are: the module of wind speed vector, the direction and vertical component (z). These values are projected  
 198 to meteorological coordinates to obtain the three components of wind speed vector (x, y, z) after being filtered the  
 199 transformation of high-frequency signals into means, variances, and covariances has been done.

200 The 10 minutes values of wind speed from sonic anemometer after applying steps 1 to 3 are checked and some  
 201 non-valid data are detected. As in conventional sensors these invalid data are due to icing effects so they are filtered.

#### 202 4.4 Stability assessment

203 MP5's sonic anemometer allowing evaluating stability based on the local Obukhov length at different heights. This  
 204 will be the benchmark method since it is directly obtained from the measurements without introducing any  
 205 assumptions or empirical relationships. The bulk Richardson number is evaluated as an alternative methodology  
 206 since it follows easier instrumentation set-up and post-processing, and for offshore places has presented good results  
 207 (Sanz Rodrigo, 2011; Sanz Rodrigo et al., 2015).

##### 208 4.4.1 Sonic method

209 To obtain the stability parameter  $\zeta = z/L$ , as it was explained before, sonic anemometer measurements are rotated to  
 210 the mean streamline coordinate system using the planar fit method to guarantee that the mean streamline plane will  
 211 be parallel to the terrain surface. After this, variances and covariances of detrended velocity and sonic temperature  
 212 perturbations are computed using the eddy covariance technique over high frequency timescale. Then, turbulent  
 213 fluxes are obtained by averaging the covariances over a period of 10 minutes.

214 In complex terrain, the hypothesis of a homogeneously horizontal surface layer is not fulfilled so the applicability of  
 215 Monin and Obukhov similarity theory (MOST) to complex terrain conditions is not obvious. This signify that for the  
 216 complex sites as Alaiz the theory is not completely valid because the topography creates local variations of wind  
 217 flow near the ground (Kaimal, 1994).

##### 218 4.4.2 Bulk Richardson number

219 As it was explained before, sonic anemometry is not routinely used in wind energy, and bulk Richardson number  $Ri_b$   
 220 is an alternative way to estimate atmospheric stability based on a temperature difference and a single velocity level.





221 In  $Ri_b$  number equation, potential temperature  $\Theta$ , is the temperature of an air parcel with absolute temperature  $T$   
222 and pressure  $p$  would have if brought adiabatically to the pressure at the 1000 mb level. To first order it can be  
223 calculated as:

$$\theta = T + \left( \frac{g}{C_p} \right) \Delta z \quad \text{Equation 5}$$

224 Where  $g$  is the acceleration due gravity,  $C_p$  is the specific heat at constant pressure, and  $\Delta z$  is the height  
225 difference from the 1000 mb level.

226 With Equation 3 the obtained  $Ri_b$  will be used to estimates the stability parameter  $\zeta = z/L$ . As Bardal *et al.*  
227 (Bardal *et al.*, 2018) explain, these formulations are only valid for values lower than 0.2, but to make a classification  
228 according to atmospheric stability they are considered adequate.

## 229 5. Results and discussion

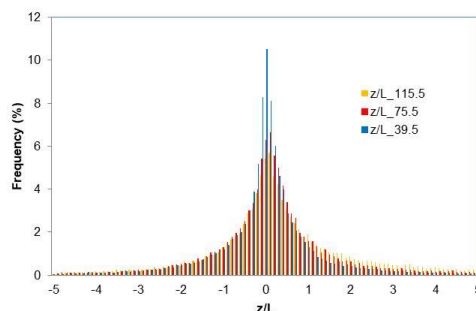
230 The study is divided into two parts: statistics of atmospheric stability with both methods (the Obukhov length and  
231 Richardson Bulk); and comparison between both methods.

### 232 5.1 Sonic method

233 Atmospheric boundary layer (ABL) models used in wind farm design tools are typically based on Monin-Obukhov  
234 theory. In stable conditions this surface-layer theory is extended to the entire ABL by assuming local scaling of  
235 turbulence characteristics through the stability parameter  $\zeta = z/L$ . This similarity theory would produce self-similar  
236 profiles of dimensionless quantities regardless of the height above ground level.

237 In the study case, as it was explained before, from the high-frequency (20 Hz) data recorded in the three  
238 available sonic anemometers in MP5 mast, the values of the Obukhov length ( $L$ ) over a period of 10 minutes have  
239 been obtained, and taking into account the heights at which they are installed, the parameter  $\zeta = z/L$ .

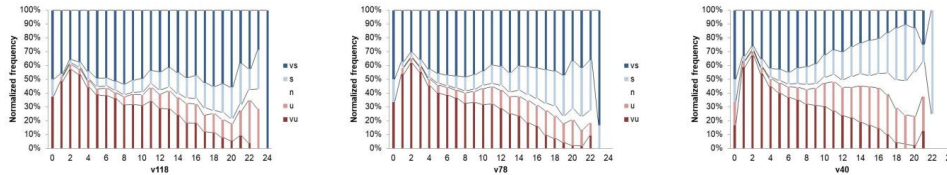
240 In Figure 4 the stability parameter  $\zeta = z/L$  frequency distribution at the three sonic heights is depicted, resulting  
241 in showing a good agreement among them with a reduction of the percentage of conditions near neutral stability as  
242 the measurement height increases.



243  
244 **Figure 4 Probability distribution of  $z/L$  at all the sonic heights. Only concurrent time steps between July 2014 and June**  
245 **2015 are included.**

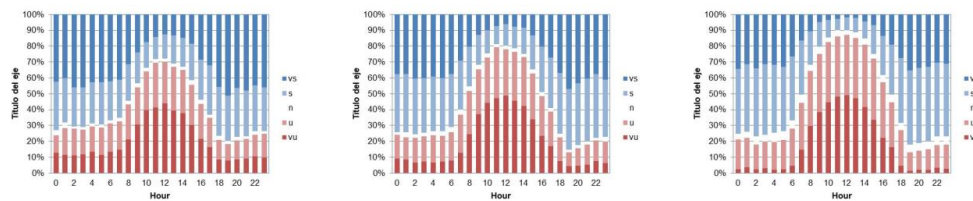
246 Figure 5 shows the distribution of atmospheric stability against wind speed at the MP5 measurements heights,  
247 the 9 stability classes propose in Table 1 are reduced to five combining: weakly un/stable classes with un/stable  
248 classes; and very un/stable with extremely un/stable. For the three heights, the stable situations are slightly higher  
249 than the unstable ones and there is an increase of neutral and stable conditions with increasing wind speeds, this is in  
250 accordance with the general knowledge that for strong wind speeds the atmosphere becomes neutrally stratified.

251 As mentioned before, it is observed a significant dependence of stability distributions with height. At higher  
252 levels, the stability distributions are broader and there are more frequent cases with very large and extreme stability.  
253 This dependency of the stability distribution with height is because  $z$  is part of the definition of the stability  
254 parameter; and closer to the ground there are more “neutral” conditions because  $z/L$  tends to zero.



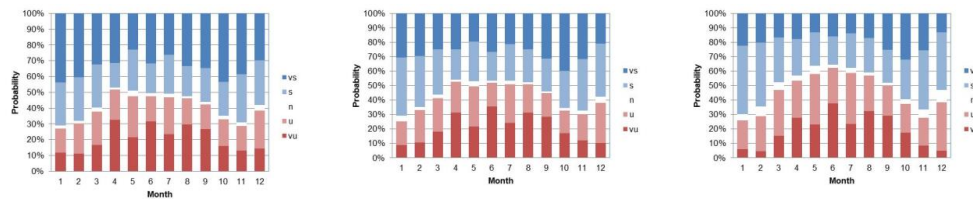
255 **Figure 5** Distribution of atmospheric stability with wind speed based on  $z/L$  obtained with sonic anemometer at different  
 256 heights, 115.5 m on the left, 75.5 m in the middle and 39.5 m on the right side. vs, very stable; s, stable; n, neutral; u,  
 257 unstable; vu, very unstable.

258 The diurnal cycle, see Figure 6, presents unstable conditions developing from 9.00 to 15.00. The rest of the day  
 259 is dominated by stable conditions resulting in low turbulence intensities.



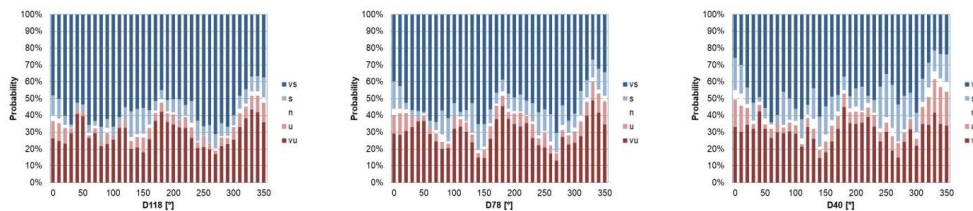
260 **Figure 6** Distribution of atmospheric stability with hour based on  $z/L$  obtained with sonic anemometer at different  
 261 heights, left 115.5 m, center 75.5 m and right 39.5 m. vs, very stable; s, stable; n, neutral; u, unstable; vu, very unstable.

262 Figure 7 shows the evolution of stability throughout the year. The stable side dominates during winter months,  
 263 with unstable conditions peaking between April to August where they take a  $\approx 50\%$  share.  
 264



265 **Figure 7** Monthly distribution of stability based on  $z/L$  obtained with sonic anemometer at different heights, left 115.5  
 266 m, center 75.5 m and right 39.5 m. vs, very stable; s, stable; n, neutral; u, unstable; vu, very unstable.

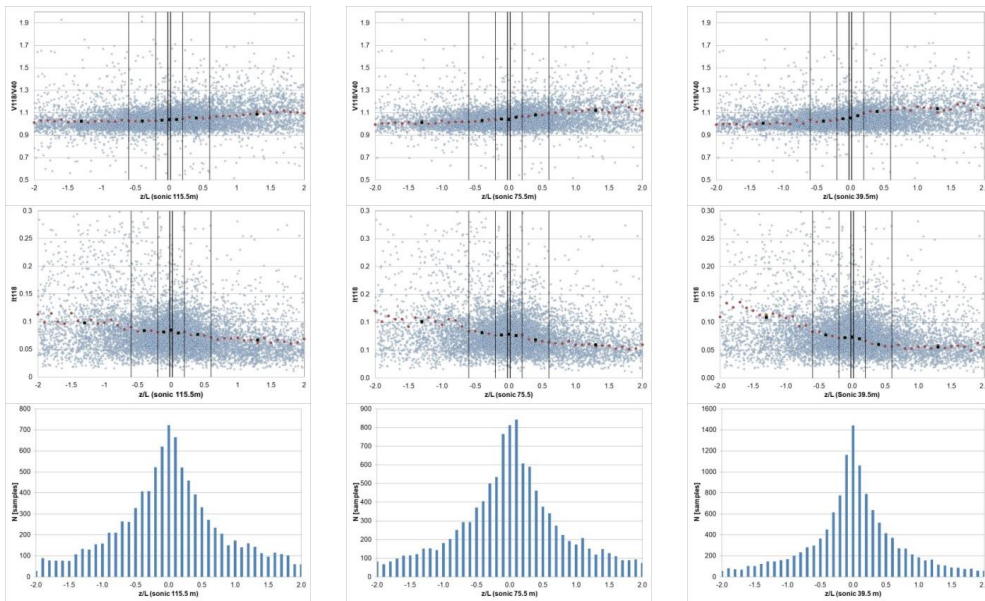
267 The variation of atmospheric stability with wind direction is shown in Figure 8. Stable situations dominate in  
 268 most of the directions except for the northwest direction ( $330^\circ$ - $350^\circ$ ) that is one of the predominant in Alaiç.



269 **Figure 8** Distribution of atmospheric stability with wind direction based on  $z/L$  obtained with sonic anemometer at  
 270 different heights. vs, very stable; s, stable; n, neutral; u, unstable; vu, very unstable.

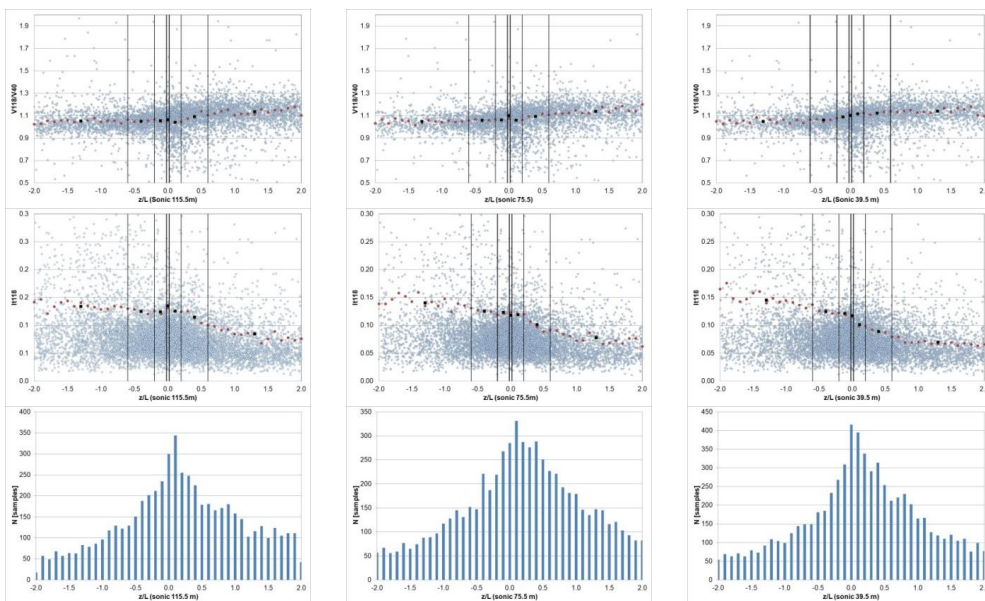
271 Following the stability classification defined in Table 1, Figure 9 and Figure 10 present the dependency of wind  
 272 shear and turbulence intensity with stability based on  $z/L$  parameter from the three sonic sensors installed for the  
 273 NNW and SSE prevailing wind direction sectors.  
 274





275 **Figure 9** Wind shear and turbulence intensity vs sonic stability in *MP5*, [337.5°-22.5°] sector. Red dots are the  $z/L$  mean  
 276 values for 0.01 resolution scale, black squares are the  $z/L$  mean values in each of the stability classes according to Table 1.

277



278 **Figure 10** Wind shear and turbulence intensity vs sonic stability in *MP5*, [157.5°-202.5°] sector. Red dots are the  $z/L$  mean  
 279 values for 0.01 resolution scale, black squares are the  $z/L$  mean values in each of the stability classes according to Table 1.

280 For the three heights is observed that, as is explained by (Stefan Emeis, 2013), in unstable situations the ground  
 281 surface is warmer than the air above so there is a positive heat flux that causes more turbulence. This results in a  
 282 convective, well-mixed, surface layer with small vertical gradients. On the other hand, lower turbulence and high  
 283 shear wind profiles are associated to stable situations where turbulence is reduced due to a negative vertical heat  
 284 flux.



## 285 5.2 Bulk Richardson number

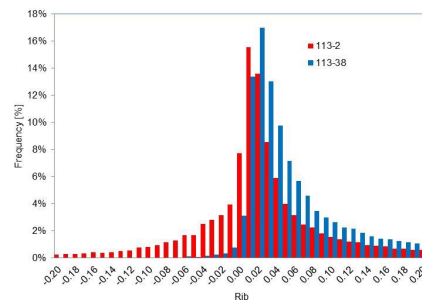
286 Since sonic anemometers are not commonly used in wind resource assessment, an alternative method to estimate the  
287 atmospheric stability is Bulk Richardson number. It is based on mean wind speed at height  $z$  and mean virtual  
288 potential temperature difference between air at the reference height ( $z$ ) and surface temperature.

289 The calculation of the Bulk–Richardson number is, in the present study, not straightforward because of the lack  
290 of reliable sensors at the surface. The lower air temperature is measured at 2 m in MP5 mast. Ideally, the  
291 temperature difference at the air–surface interface is required (Kaimal, 1994) for stability analysis. However,  
292 because of the lack of surface temperature, 2 m height air temperature has been chosen as representative.  
293 Observations of 118 m wind speed and 113 m air temperature have been used in conjunction with 2 m air  
294 temperature to estimate  $Ri_b$ .

295 As in the work that is presented in some measurement campaigns, there are no measurements of surface  
296 temperature or near the ground. Some authors in these circumstances either extrapolate the values to the surface  
297 ( $z=0$ ) (Machefaux et al., 2016) or perform the calculation directly between the available temperature levels (Martin  
298 et al., 2016; Ruisi y Bossanyi, 2019; Zhan et al., 2020). To analyze how the choice of measurement heights may  
299 influence resulting  $Ri_b$  stability distributions the  $Ri_b$  has also been calculated using 38 m air temperature instead 2 m.

300 Figure 11 shows the distribution for the bulk Richardson number method. The lower measurement level is varied  
301 between 2 and 38 m. Using the 38 m level, it is observed that according to the classification in Table 2, unstable  
302 cases practically disappear. This is not physically possible and does not occur in the classification obtained by the  
303 sonic method (see Figure 4). So In this case, the results obtained using the 38 m temperature sensor as a  
304 representative surface level does not give us any reliable information. Small temperature differences highly affect  
305 the result of the Richardson number method and therefore it is greatly affected by deviations in the measurement of  
306 this variable. The MP5 temperature sensors have an accuracy of 0.3°C and the mean temperature difference in the  
307 period analyzed between the level of 38m and that of 113 has been 0.7°C so the uncertainty of the measurement is of  
308 the same order as the measurement itself.

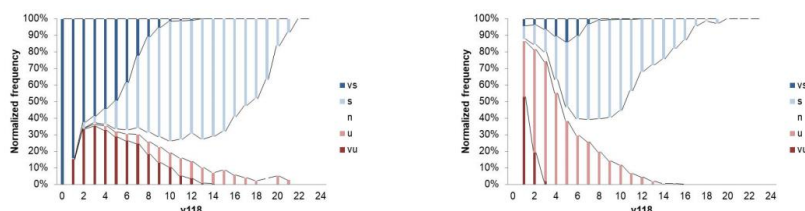
309 The selection of temperature measurement heights has a great effect on the bulk Richardson number method,  
310 both in the exactitude and in the applicability of the method. To reduce uncertainties the measurements should be  
311 made either with differential temperature sensors or with calibrated sensors and a sufficient vertical separation in  
312 order to reduce the influence of inaccuracies in the temperature measurements.



313  
314 **Figure 11 Probability distribution of  $Ri_b$  measured between 2 m and 113 (red one) and between 38 and 113 m (blue lines).**  
315 **Only concurrent time steps between July 2014 and June 2015 are included.**

316  
317 Figure 12 shows the distribution of atmospheric stability against wind speed. On the left side atmospheric  
318 stability is directly classified with the  $Ri_b$  obtained with observations of 118 m wind speed, 113 m air temperature  
319 and 2 m air temperature, this last temperature sensor has been chosen as representative of surface temperature. The  
320 seven stability classes propose in Table 2 are reduced to five combining: weakly un/stable classes with un/stable  
321 classes. On the right side atmospheric stability is classified according to the stability parameter  $\zeta = z/L$  obtained with  
322  $Ri_b$  and Equation 3. The nine stability classes propose in Table 1 are reduced to five combining: weakly un/stable  
323 classes with un/stable classes; and very un/stable with extremely un/stable.

324 Both distributions show a differentiated behavior with fewer “very” un/stable situations and a greater number of  
325 neutral observations in the case of the classification with  $\zeta$  (on the right side of Figure 12).



326 **Figure 12** Distribution of atmospheric stability with wind speed. On the left based on  $Ri_b$ ; On the right based on  $z/L$   
 327 obtained from  $Ri_b$  with transformation functions by Businger and Dyer. vs, very stable; s, stable; n, neutral; u,  
 328 unstable; vu, very unstable.

329 **5.3 Comparison of stability methods: sonic versus bulk method**

330 Comparing the distribution of atmospheric stability against wind speed based on sonic method (Figure 5) with the  
 331 results obtained based on  $Ri_b$  method (Figure 12); it is observed that there are important differences between them.

332 Table 3 presents a frequency of occurrence of stability classes with concurrent data using different methods. This  
 333 quantitative comparison shows that taking the sonic method as benchmark, it is observed that the bulk method when  
 334 the Businger and Dyer functions are used to estimate the stability parameter  $\zeta = z/L$  over predict the percentage of  
 335 neutral and stable conditions to the detriment of very un/stable situations, probably due to similar air temperature  
 336 values at 113 an 2 m. On the other hand, classification directly with  $Ri_b$  according to Mohan classification over  
 337 predict too the stable situations at the cost of under predicting the unstable ones. As is explained in some references  
 338 (Bardal et al., 2018; Sathe et al., 2011), stability characterization with  $Ri_b$  have several weak points: in one hand  $Ri_b$   
 339 method is sensitive to temperature measurements and uncertainty in L estimation increases as the temperature  
 340 difference is reduced. Besides, other source of uncertainty comes from the definition of the surface temperature. In  
 341 the other hand Businger and Dyer functions have some limitations and as Bardal et al. propose in (Bardal et al.,  
 342 2018) the use of more advanced methods for relating the  $Ri_b$  to de  $z/L$  parameter might improve the results.

343 Besides these methodological reasons there are some physical causes of the differences found. One of these is  
 344 that Richardson bulk number represents a bulk average stability value instead a local measurement like the sonic  
 345 method.

346

**Table 3** Frequency of occurrence of stability classes.

	115.5/L	75.5/L	39.5/L	$z/L$ from $Ri_b$	$Ri_b$
vu	21.2%	21.3%	19.9%	0.7%	18.1%
u	19.4%	21.4%	26.8%	21.2%	5.9%
n	2.2%	2.4%	4.4%	32.5%	8.2%
s	24.0%	28.2%	29.9%	42.2%	43.6%
vs	33.2%	26.7%	19.1%	3.5%	24.2%

347 **6. Conclusions**

348 In this work, a detailed data analysis focused on how to estimate atmospheric stability in a site with complex terrain  
 349 was presented. The Obukhov parameter  $\zeta = z/L$ , which can be measured locally with the use of a sonic anemometer,  
 350 and bulk Richardson number have been studied. The methods are examined considering their theoretical  
 351 background, implementation complexity, instrumentation requirements, and practical use in connection with wind  
 352 energy applications.

353 It is shown that the resulting stability depends on which method is chosen. The sonic method is taking as  
 354 benchmark because is the only way of measuring local stability without the use of empirical functions or theoretical  
 355 assumptions. However this method requires working with accurate high frequency data, rotating the measurements  
 356 to align the coordinate system to the mean wind vector, which is reported to require special attention in complex  
 357 terrain to guarantee that the mean streamline plane will be parallel to the terrain surface; to finally obtain turbulent  
 358 fluxes using the eddy covariance technique.

359 According to the stability parameter  $\zeta = z/L$  obtained with the three sonic anemometer installed in MP5 mast.  
 360 For the three heights, the stable situations are slightly higher than the unstable ones and there is an increase of



361 neutral and stable conditions with increasing wind speeds. There is a significant dependence of stability distributions  
362 with height. At higher levels, the stability distributions are broader and there are more frequent cases with very large  
363 and extreme stability.

364 The seasonal and diurnal cycle is identified, in the winter and during the hours between 17h to 8h stable side  
365 dominates, while between April to August and between 9h to 15h unstable conditions are found to be more frequent.  
366 Winds from the predominant northwest direction (330°-350°) produce more unstable conditions than the others  
367 sectors.

368 For the three heights, and in the two predominant sectors, is observed that in unstable situations the ground  
369 surface is warmer than the air above so there is a positive heat flux that causes more turbulence. This results in a  
370 convective, well-mixed, surface layer with small vertical gradients. On the other hand, lower turbulence and high  
371 shear wind profiles are associated to stable situations where turbulence is reduced due to a negative vertical heat  
372 flux.

373 As alternative to characterize stability, the bulk Richardson number is explored, it requires the minimum level of  
374 instrumentation, mean wind speed at height  $z$  and mean virtual potential temperature difference between air at the  
375 reference height ( $z$ ) and surface temperature. The bulk Richardson number can be used directly to classified the  
376 atmospheric stability or it can be transform into  $\zeta = z/L$  by Businger and Dyer functions.

377 On MP5 there is not a surface temperature sensor so 2 m high air temperature sensor has been chosen as  
378 representative, moreover to analyze how the choice of measurement heights may influence resulting  $Ri_b$  stability  
379 distributions, it has also been calculated using 38 m air temperature sensor instead 2 m. This configuration does not  
380 give us any reliable information, it could be due temperature sensors on MP5 have an accuracy of 0.3°C and the  
381 mean temperature difference in the period analyzed between the level of 38 m and that of 113 has been 0.7°C so the  
382 uncertainty of the measurement is of the same order as the measurement itself. The  $Ri_b$  number relies on smaller  
383 temperature differences for estimation of the mean gradient and its accuracy is therefore dependent on the sensor  
384 precision, calibration and measurement heights.

385 On the other hand, the stability classification obtained using directly the  $Ri_b$  values shows a differentiated  
386 behavior than that estimated according to the stability parameter  $\zeta = z/L$  obtained with  $Ri_b$  and Businger and Dyer  
387 functions. It could be by the different classification employed in both characterization (Mohan vs Sorbjan &  
388 Grachev) and/or by the Businger and Dyer functions.

389 In summary the sonic method is more costly and complex but, in this study, it shows results in accordance with  
390 the general atmospheric boundary layer knowledge. For the Bulk Richardson number, based in the references read,  
391 there isn't a standard methodology for characterizing atmospheric stability using this method and there are many  
392 different approximations. Furthermore, empirical relations to relate  $Ri_b$  to  $\zeta = z/L$  are obtained either for offshore  
393 sites or for non-complex sites, so there is a need for observational studies on complex terrain to increase under-  
394 standing of how estimate atmospheric stability accurately.

395 **Data availability.** Data belongs to CENER and it could be obtained from the author upon request.

396 **Author contribution.** EC is the principal investigator of the project and coordinated the activities and the  
397 preparation of the paper. DP aided in the formulation of the scope of the work, FB assisted in the measurement post-  
398 processing, while the methodology was devised by EC, JS and DP. The stability analysis and visualization was  
399 performed by EC. EC wrote the original draft, AG helped with the composition of the manuscript while EC, JSR,  
400 FB, DP and AG contributed, reviewed and edited the final paper.

401 **Competing interests.** The authors declare that they have no conflict of interest.

402 **Acknowledgements.** The authors are grateful to CENER for sharing the MP5 database and to

## 403 References

- 404 Abkar, M. y Porté-Agel, F.: Influence of atmospheric stability on wind-turbine wakes: A large-eddy simulation  
405 study, *Phys. Fluids*, 27(3), 35104, doi:10.1063/1.4913695, 2015.
- 406 Aubinet, M., Vesala, T. y Papale, D.: *Eddy Covariance : A practical guide to measurement and data analysis.*, 2012.
- 407 Bardal, L. M., Onstad, A. E., Sætran, L. R. y Lund, J. A.: Evaluation of methods for estimating atmospheric stability  
408 at two coastal sites, *Wind Eng.*, 42(6), 561-575, doi:10.1177/0309524X18780378, 2018.
- 409 Barthelmie, R. J.: The effects of atmospheric stability on coastal wind climates, *Meteorol. Appl.*, 6(1), 39-47,  
410 doi:10.1017/S1350482799000961, 1999.



- 411 Brower, M. C.: WIND RESOURCE ASSESSMENT: A Practical Guide to Developing a Wind Project., 2012.
- 412 Burba, G.: Eddy Covariance Method for Scientific, Industrial, Agricultural and Regulatory Applications., 2013.
- 413 Burba, G. y Anderson, D.: Eddy Covariance Flux Measurements. [en línea] Available from:  
414 <http://www.ncbi.nlm.nih.gov/pubmed/18767616>, 2010.
- 415 Businger, J. A., Wyngaard, J. C. y Izumi, Y.: Flux-Profile Relationships in the Atmospheric Surface Layer, J.  
416 Atmos. Sci, 28, 181-189, 1971.
- 417 Cuerva, A., Sanz-Andrés, A. y Navarro, J.: On multiple-path sonic anemometer measurement theory, Exp. Fluids,  
418 34(3), 345-357, doi:10.1007/s00348-002-0565-x, 2003.
- 419 Dyer, A. J.: A review of flux-profile relationships, Boundary-Layer Meteorol., 7(3), 363-372,  
420 doi:10.1007/BF00240838, 1974.
- 421 Finnigan, J., Ayotte, K., Harman, I., Katul, G., Oldroyd, H., Patton, E., Poggi, D., Ross, A. y Taylor, P.: Boundary-  
422 Layer Flow Over Complex Topography, Boundary-Layer Meteorol., 177(2-3), 247-313, doi:10.1007/s10546-020-  
423 00564-3, 2020.
- 424 Foken, T.: 50 years of the Monin-Obukhov similarity theory, Boundary-Layer Meteorol., 119(3), 431-447,  
425 doi:10.1007/s10546-006-9048-6, 2006.
- 426 Geissbühler, P., Siegwolf, R. y Eugster, W.: Eddy Covariance Measurements On Mountain Slopes: The Advantage  
427 Of Surface-Normal Sensor Orientation Over A Vertical Set-Up, Boundary-Layer Meteorol., 96(3), 371-392,  
428 doi:10.1023/A:1002660521017, 2000.
- 429 Grachev, A. A. y Fairall, C. W.: Dependence of the M-O stability parameters on the Bulk Ri over the ocean JAM  
430 36.pdf, J. Appl. Meteorol., 36, 406-415, doi:10.1175/1520-0450(1997)036<0406:DOTMOS>2.0.CO;2, 1997.
- 431 Han, X., Liu, D., Xu, C. y Shen, W. Z.: Atmospheric stability and topography effects on wind turbine performance  
432 and wake properties in complex terrain, Renew. Energy, 126, 640-651, doi:10.1016/j.renene.2018.03.048, 2018.
- 433 Hansen, K. H., Barthelmie, R. J., Jensen, L. E. y Sommer, A.: The impact of turbulence intensity and atmospheric  
434 stability on power deficits due to wind turbine wakes at Horns Rev wind farm., Wind Energy, 15, 183-196, 2010.
- 435 IEC61400-1 (ED4) 2019: Wind energy generation systems - Part 1: Design requirements. [en línea] Available from:  
436 <https://webstore.iec.ch/publication/26423> (Accedido 16 abril 2021), 2019.
- 437 IEC61400-12-1 (ED1) 2005-12: Wind turbines- Part 12-1: Power performance measurements of electricity  
438 producing wind turbines., 2005.
- 439 Kaimal, J. C. y Businger, J. a.: A Continuous Wave Sonic Anemometer-Thermometer, J. Appl. Meteorol., 2(1), 156-  
440 164, doi:10.1175/1520-0450(1963)002<0156:ACWSAT>2.0.CO;2, 1963.
- 441 Kaimal, J. C. y Gaynor, J. E.: Another look at sonic thermometry, Boundary-Layer Meteorol., 56(4), 401-410,  
442 doi:10.1007/BF00119215, 1991.
- 443 Kaimal, J. C. J. J. F.: Atmospheric Boundary Layer Flows: Their Structure and Measurement, 1.<sup>a</sup> ed., Oxford  
444 University Press., 1994.
- 445 Kelly, M., Larsen, G., Dimitrov, N. K. y Natarajan, A.: Probabilistic Meteorological Characterization for Turbine  
446 Loads, J. Phys. Conf. Ser., 524, 012076, doi:10.1088/1742-6596/524/1/012076, 2014.
- 447 Lange, B., Larsen, S., Højstrup, J. y Barthelmie, R.: Importance of thermal effects and sea surface roughness for  
448 offshore wind resource assessment, J. Wind Eng. Ind. Aerodyn., 92(11), 959-988, doi:10.1016/j.jweia.2004.05.005,  
449 2004a.
- 450 Lange, B., Larsen, S., Højstrup, J. y Barthelmie, R.: The Influence of Thermal Effects on the Wind Speed Profile of  
451 the Coastal Marine Boundary Layer, Boundary-Layer Meteorol., 112(3), 587-617,  
452 doi:10.1023/B:BOUN.0000030652.20894.83, 2004b.
- 453 Machefaux, E., Larsen, G. C., Koblitz, T., Troldborg, N., Kelly, M. C., Chougule, A., Hansen, K. S. y Rodrigo, J.  
454 S.: An experimental and numerical study of the atmospheric stability impact on wind turbine wakes, Wind Energy,  
455 19(10), 1785-1805, doi:<https://doi.org/10.1002/we.1950>, 2016.
- 456 Martin, C. M. S., Lundquist, J. K., Clifton, A., Poulos, G. S. y Schreck, S. J.: Wind turbine power production and  
457 annual energy production depend on atmospheric stability and turbulence, Wind Energy Sci., 1(2), 221-236,  
458 doi:10.5194/wes-1-221-2016, 2016.
- 459 Measnet: ANEMOMETER CALIBRATION Version 2 October 2009, Measurement, (October) [en línea] Available





- 460 from: [http://www.measnet.com/wp-content/uploads/2011/06/measnet\\_anemometer\\_calibration\\_v2\\_oct\\_2009.pdf](http://www.measnet.com/wp-content/uploads/2011/06/measnet_anemometer_calibration_v2_oct_2009.pdf),  
461 2009.
- 462 Mohan, M.: Analysis of various schemes for the estimation of atmospheric stability classification, *Atmos. Environ.*,  
463 32(21), 3775-3781, doi:10.1016/S1352-2310(98)00109-5, 1998.
- 464 Monin, A. S. y Obukhov, A. M.: Basic laws of turbulent mixing in the atmosphere near the ground, *Tr. Akad. Nauk*  
465 *SSSR Geofiz. Inst.*, 24, 163-187, 1954.
- 466 Nieuwstadt, F. T. M.: The turbulent structure of the stable, nocturnal boundary layer., *J. Atmos. Sci.*, 41(14), 2202-  
467 2216, doi:10.1175/1520-0469(1984)041<2202:TTSOTS>2.0.CO;2, 1984.
- 468 Peña, A. y Hahmann, A. N.: Atmospheric stability and turbulence fluxes at Horns Rev—an intercomparison of  
469 sonic, bulk and WRF model data, *Wind Energy*, 15(5), 717-731, doi:<https://doi.org/10.1002/we.500>, 2012.
- 470 Radünz, W. C., Sakagami, Y., Haas, R., Petry, A. P., Passos, J. C., Miqueletti, M. y Dias, E.: The variability of wind  
471 resources in complex terrain and its relationship with atmospheric stability, *Energy Convers. Manag.*, 222(July),  
472 113249, doi:10.1016/j.enconman.2020.113249, 2020.
- 473 Radünz, W. C., Sakagami, Y., Haas, R., Petry, A. P., Passos, J. C., Miqueletti, M. y Dias, E.: Influence of  
474 atmospheric stability on wind farm performance in complex terrain, *Appl. Energy*, 282(PA), 116149,  
475 doi:10.1016/j.apenergy.2020.116149, 2021.
- 476 Richiardone, R., Giampiccolo, E., Ferrarese, S. y Manfrin, M.: Detection of Flow Distortions and Systematic Errors  
477 in Sonic Anemometry Using the Planar Fit Method, *Boundary-Layer Meteorol.*, 128(2), 277-302,  
478 doi:10.1007/s10546-008-9283-0, 2008.
- 479 Ruisi, R. y Bossanyi, E.: Engineering models for turbine wake velocity deficit and wake deflection. A new proposed  
480 approach for onshore and offshore applications, *J. Phys. Conf. Ser.*, 1222(1), doi:10.1088/1742-  
481 6596/1222/1/012004, 2019.
- 482 Santos, P., Mann, J., Vasiljević, N., Cantero, E., Sanz Rodrigo, J., Borbón, F., Martínez-Villagrasa, D., Martínez,  
483 B. y Cuxart, J.: The Alaiz experiment: untangling multi-scale stratified flows over complex terrain, *Wind Energy*  
484 *Sci.*, 5(4), 1793-1810, doi:10.5194/wes-5-1793-2020, 2020.
- 485 Sanz Rodrigo, J.: Flux-profile characterization of the offshore ABL for the parameterization of CFD models, *EWEA*  
486 offshore, 2011.
- 487 Sanz Rodrigo, J., Borbón Guillén, F., Gómez Arranz, P., Courtney, M. S., Wagner, R. y Dupont, E.: Multi-site  
488 testing and evaluation of remote sensing instruments for wind energy applications, *Renew. Energy*, 53, 200-210,  
489 doi:10.1016/j.renene.2012.11.020, 2013.
- 490 Sanz Rodrigo, J., Cantero, E., García, B., Borbón, F., Irigoyen, U., Lozano, S., Fernandez, P. M. y Chávez, R. A.:  
491 Atmospheric stability assessment for the characterization of offshore wind conditions, *J. Phys. Conf. Ser.*, 625,  
492 012044, doi:10.1088/1742-6596/625/1/012044, 2015.
- 493 Sathe, A., Gryning, S.-E. y Peña, A.: Comparison of the atmospheric stability and wind profiles at two wind farm  
494 sites over a long marine fetch in the North Sea, *Wind Energy*, 14(6), 767-780, doi:10.1002/we.456, 2011.
- 495 Sathe, A., Mann, J., Barlas, T., Bierbooms, W. A. A. M. y van Bussel, G. J. W.: Influence of atmospheric stability  
496 on wind turbine loads, *Wind Energy*, 16(7), 1013-1032, doi:<https://doi.org/10.1002/we.1528>, 2013.
- 497 Schmidt, J., Chang, C.-Y., Dörenkämper, M., Salimi, M., Teichmann, T. y Stoevesandt, B.: The consideration of  
498 atmospheric stability within wind farm AEP calculations, *J. Phys. Conf. Ser.*, 749, 012002, doi:10.1088/1742-  
499 6596/749/1/012002, 2016.
- 500 Schotanus, P., Nieuwstadt, F. T. M. y Bruin, H. A. R.: Temperature measurement with a sonic anemometer and its  
501 application to heat and moisture fluxes, *Boundary-Layer Meteorol.*, 26(1), 81-93, doi:10.1007/BF00164332, 1983.
- 502 Sorbjan, Z. y Grachev, A. A.: An Evaluation of the Flux--Gradient Relationship in the Stable Boundary Layer,  
503 *Boundary-Layer Meteorol.*, 135(3), 385-405, doi:10.1007/s10546-010-9482-3, 2010.
- 504 Stefan Emeis: *Wind Energy Meteorology Atmospheric Physics for Wind Power Generation (Green Energy and*  
505 *Technology)*, First Edit., Springer, Berlin, Heidelberg., 2013.
- 506 Stiperski, I. y Rotach, M. W.: On the Measurement of Turbulence Over Complex Mountainous Terrain, *Boundary-*  
507 *Layer Meteorol.*, 159(1), 97-121, doi:10.1007/s10546-015-0103-z, 2015.
- 508 Stull, R. B.: *An Introduction to Boundary Layer Meteorology*, Springer Netherlands., 1989.





- 509 Westerhellweg, A., Cañadillas, B., Kinder, F. y Neumann, T.: Wake measurements at alpha ventus - Dependency on  
510 stability and turbulence intensity, *J. Phys. Conf. Ser.*, 555(1), doi:10.1088/1742-6596/555/1/012106, 2014.
- 511 Wilczak, J. M., Oncley, S. P. y Stage, S. A.: Sonic Anemometer Tilt Correction Algorithms, *Boundary-Layer*  
512 *Meteorol.*, 99(1), 127-150, doi:10.1023/A:1018966204465, 2001.
- 513 Zhan, L., Letizia, S. y Valerio Iungo, G.: LiDAR measurements for an onshore wind farm: Wake variability for  
514 different incoming wind speeds and atmospheric stability regimes, *Wind Energy*, 23(3), 501-527,  
515 doi:<https://doi.org/10.1002/we.2430>, 2020.
- 516